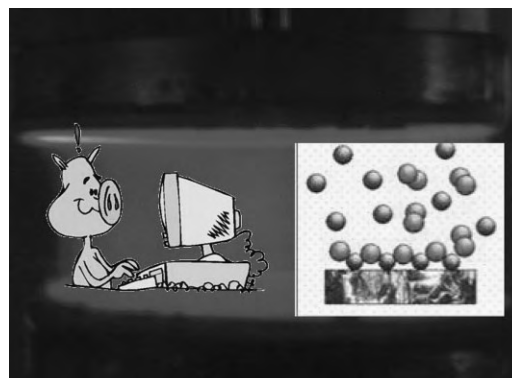


Computer Modeling of Plasmas and Plasma-Surface Interactions

Annemie Bogaerts,* Evi Bultinck, Maxie Eckert, Violeta Georgieva, Ming Mao, Erik Neyts, Laurent Schwaederlé

In this paper, an overview is given of different modeling approaches used for describing gas discharge plasmas, as well as plasma-surface interactions. A fluid model is illustrated for describing the detailed plasma chemistry in capacitively coupled rf discharges. The strengths and limitations of Monte Carlo simulations and of a particle-in-cell–Monte Carlo collisions model are explained for a magnetron discharge, whereas the capabilities of a hybrid Monte Carlo–fluid approach are illustrated for a direct current glow discharge used for spectrochemical analysis of materials. Finally, some examples of molecular dynamics simulations, for the purpose of plasma-deposition, are given.



Introduction

There exist several approaches in literature to model gas discharge plasmas, including analytical models,^[1] fluid models,^[2] the Boltzmann transport equation,^[3] Monte Carlo (MC)^[4] and particle-in-cell–Monte Carlo collisions (PIC-MCC) simulations,^[5] and hybrid modeling networks, consisting of different kinds of models, such as fluid and Monte Carlo simulations.^[6] All these modeling approaches have their specific advantages and limitations, and therefore, the choice of the model is often dictated by the gas discharge and conditions under study. This will be illustrated below, with some examples of modeling activities, currently going on in our research group. Furthermore, besides the plasma processes themselves, a better understanding of the interaction of the plasma species with the surface is also of great importance, because it determines the boundary conditions of the

plasma modeling, and also because it forms the basis of many applications, such as thin film deposition, surface etching, modification, etc. Therefore, besides modeling of the plasma behavior itself, some examples will also be given here of molecular dynamics (MD) simulations carried out in our research group, to describe plasma-surface interactions for thin film deposition purposes.

Fluid Modeling

Fluid modeling is based on solving the continuity and transport equations (often based on diffusion and migration) for the various plasma species, in combination with Poisson equation, in order to obtain a self-consistent electric field distribution. This approach is particularly suitable for describing the detailed plasma chemistry, as will be illustrated here for capacitively coupled (cc) rf discharges in C₂H₂. Indeed, a large number of different plasma species and chemical reactions can be included in the model, without too much computational effort. In the case of a C₂H₂ plasma, 78 different species (i.e., molecules, radicals, positive and negative ions, up to a maximum of 12 C-atoms, as well as the electrons) were included in the

A. Bogaerts, E. Bultinck, M. Eckert, V. Georgieva, M. Mao, E. Neyts, L. Schwaederlé

Research group PLASMANT, Department of Chemistry, University of Antwerp, Universiteitsplein 1, B-2610 Wilrijk-Antwerp, Belgium
E-mail: annemie.bogaerts@ua.ac.be



Annemie Bogaerts studied chemistry at the University of Antwerp. She received her M.Sc. degree in 1993 and her PhD degree in 1996. Since 2003, she is a professor of physical chemistry at the University of Antwerp, and head of the research group PLASMANT. Her research interests are computer modeling of various kinds of plasmas, plasma-surface interactions and laser-surface interactions.



Evi Bultinck received her M.Sc. degree in chemistry at the University of Antwerp in 2005. She is currently working towards a Ph.D. degree, on particle-in-cell/Monte Carlo modeling of magnetron discharges in Ar/N₂ and Ar/O₂, for the reactive sputter-deposition of nitride and oxide layers.



Maxie Eckert received the M.Sc. degree in chemistry from the University of Antwerp, 2006. Currently, she investigates the growth of (ultra)nanocrystalline diamond by molecular dynamics and Monte Carlo simulations, working toward the Ph.D. degree at the University of Antwerp.



Violeta Georgieva graduated as M.Sc. in physics at Sofia University, Bulgaria. She received her Ph.D. degree from the University of Antwerp, Belgium, in 2006 for her work on PIC/MCC modeling of fluorocarbon-based discharges. Her current research includes molecular dynamics simulations of metal-oxide thin film deposition.



Ming Mao obtained his Ph.D. in plasma physics at Dalian University of Technology in P. R. China. He currently works as a postdoc in the PLASMANT research group to study the plasma chemistry of hydrocarbon-based plasmas, used for applications of carbon-nanomaterials, by fluid modeling.



Erik Neyts studied chemistry at the University of Antwerp. He obtained his M.Sc. degree in 2001, and finished his Ph.D. in March 2006 on molecular dynamics simulations for the deposition of diamond-like carbon layers. Since then, he works as a postdoc, first on molecular dynamics and fluid dynamics simulations for metal oxide deposition, and since October 2007, on molecular dynamics and Monte Carlo simulations for the growth of carbon nanostructured materials.



Laurent Schwaederlé got his master in plasma physics and his Ph.D. in fluid mechanics (France). He worked in C.E.A. (France) on shock induced instability, and later on in the C.A.P.S.T. lab (South Korea) on the development of optimized magnetron sources. He works currently in the research group PLASMANT on magnetron modeling (particle/Monte-Carlo modeling).

model, and around 400 chemical reactions were taken into account. More details of the species and reactions included in the model can be found in ref. [7] By comparing with experimental data, for instance mass spectra, some knowledge can be obtained on the relative importance of certain mechanisms, as illustrated below. Figure 1 and 2 illustrate a comparison between our calculated species intensities (based on the fluxes towards the electrode) and mass spectral intensities, for positive and negative ions, respectively. It is clear that the mass spectra, as measured by Deschenaux et al.^[8] contain much more peaks than the simulated spectra, illustrating that a lot of different species are present in the plasma. However, the most important peaks are also found back in the simulated spectra, and the relative intensities show very similar trends. This is especially true for the positive ions (see Figure 1). For the negative ions (Figure 2), the agreement is slightly worse, but still very reasonable. Indeed, the C₆H⁻ ion is found to be the dominant negative ion, whereas in our previous model for a C₂H₂ plasma,^[9] the C₂H⁻ ion appeared to have the largest intensity and a decreasing trend towards larger negative ions was predicted.^[9] This illustrates that some mechanisms were at that point not yet included in our model, which turn out to be important in the plasma. These new mechanisms were proposed in our recent paper.^[7] Indeed, in our previous model only the so-called Winchester mechanism^[10] was included for anion growth, i.e., the primary C₂H⁻ ions, generated through electron impact dissociative attachment on C₂H₂, can trigger a consecutive chain of polymerization reactions with C₂H₂ insertion to form larger anions C_{2n}H⁻ (n = 2–6). However, this yields the decreasing trend towards larger anions, as shown in ref. [9] Therefore, a new mechanism was proposed,^[7] based on dissociative electron attachment to larger hydrocarbon molecules (C_{2n}H₂; n = 2–5), and more specifically to branched C_{2n}H₂ molecules (n > 2). These branched molecules are suggested to be formed in the polymerization process of C_{2n}H₂ growth, where the C₂H radical is not only attached to the end C-atoms (yielding linear structures) but also to the middle C-atoms, giving rise to branched molecules. Assuming that these branched molecules are characterized by a higher reactivity, giving enhanced dissociative electron attachment, this can explain why the C₆H⁻ ions have the highest intensity (see ref. [7] for a more detailed discussion). This example illustrates that the detailed plasma chemistry can be investigated via fluid modeling, and new mechanisms can be proposed, by comparing with experimental data. Such investigations are important, as these reactions are considered as the initial mechanisms towards nanoparticle formation and growth in C₂H₂ plasmas. It should, however, be mentioned that, when investigating detailed plasma chemistry, the weak point of fluid modeling (and modeling in general) is the lack of suitable data for the rate

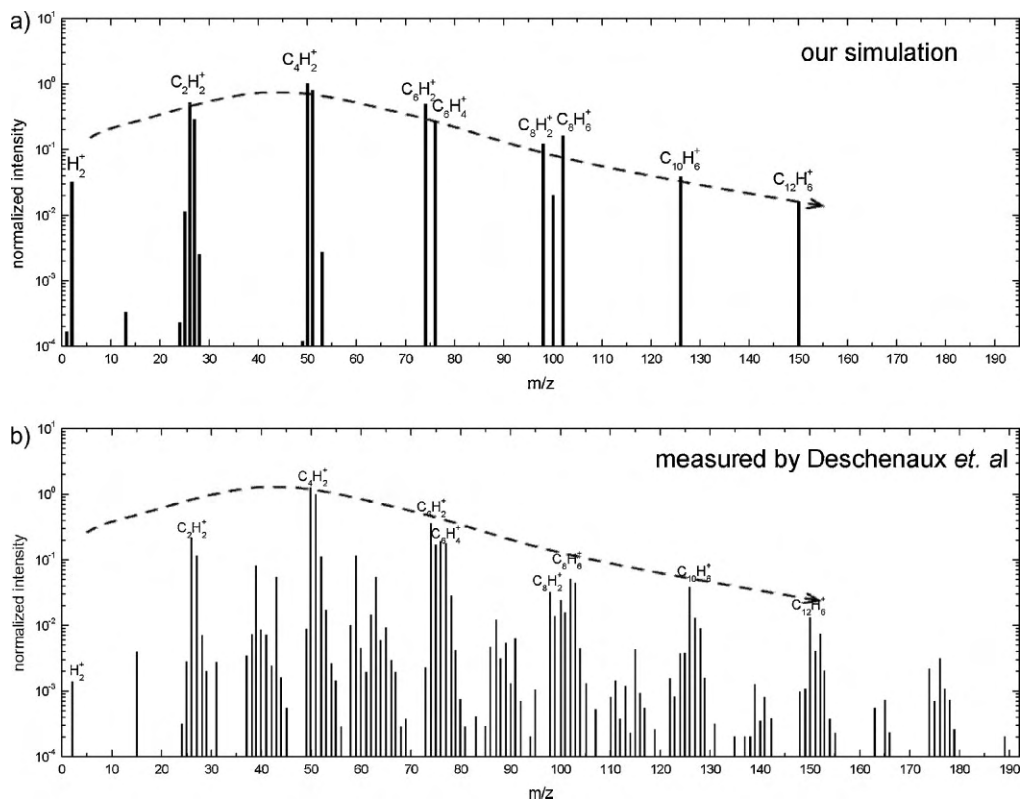


Figure 1. Calculated a) and measured b) mass spectra of the positive ions in a capacitively coupled radiofrequency discharge, operating in acetylene at 27 Pa, 13.56 MHz and 40 W (adopted from ref. [7] with kind permission of IOP Publishing).

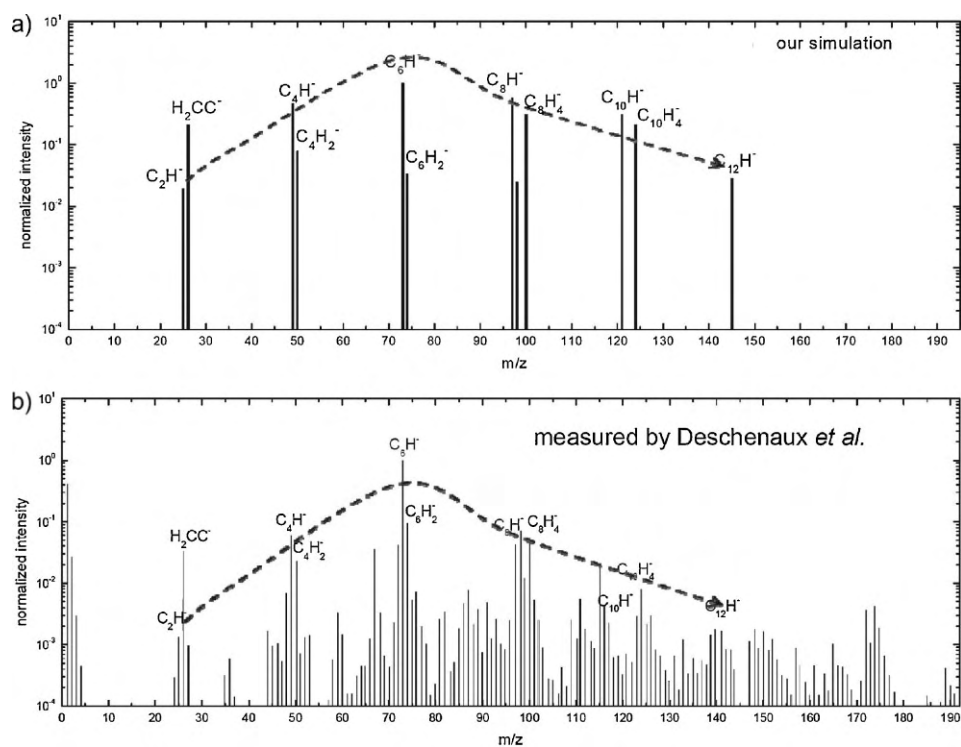


Figure 2. Calculated a) and measured b) mass spectra of the negative ions in a capacitively coupled radiofrequency discharge, operating in acetylene at 27 Pa, 13.56 MHz and 40 W (Adopted from ref. [7] with kind permission of IOP Publishing).

constants of all chemical reactions included in the model. Therefore, assumptions often have to be made, based on similar reactions and comparison with experiment. This clearly shows the need of more complete databases for modeling. Another weak point of fluid modeling is that it assumes that the energy of the plasma species, gained by the electric field, is more or less balanced by their energy lost as a result of collisions in the plasma. For the heavy particles, such as ions, and certainly for the neutral species (molecules, radicals) which do not gain energy from the electric field, this is a good approximation, but on the other hand, the electrons typically gain more energy from the electric field than they lose by collisions, especially in the case of low pressures. The electron energy is often calculated in fluid modeling by solving an energy balance equation, but this yields only the mean electron energy, whereas in reality, electrons can have energies ranging from thermal to high energies, corresponding to the discharge voltage. This electron energy can be calculated more accurately in Monte Carlo (MC) simulations, as illustrated below.

Monte Carlo (MC) Simulations

The example shown here describes magnetron discharges used for sputter-deposition applications. The electrons are trapped in the magnetic field, and give rise to enhanced ionization in the plasma, due to their longer path lengths. The behavior of the electrons in the plasma can very well be described with MC simulations. Indeed, the detailed trajectory of individual electrons, under the influence of the electric and magnetic field, is calculated with Newton's laws. The collisions (i.e., occurrence of a collision, kind of collision, and new energy and direction after collision) are treated with random numbers. By following in this way a large number of individual electrons, their behavior can be statistically simulated. Figure 3 illustrates the trajectory of one electron as a function of time, starting from its emission from the cathode (target) until it escapes the magnetic trap, for an unbalanced circular planar magnetron reactor, in side view a) and perspective view b). The electron starting position is indicated in Figure 3b by a small arrow. The computational volume is a cylinder with the same diameter as the target diameter (50 mm) and a height of 20 mm. The static magnetic flux density is calculated in a full 3D configuration using the Open Source finite element solver GetDP^[11] to solve the magnetostatic equations, together with the three-dimensional finite element mesh generator Gmsh.^[12] The calculated B magnetic field is indicated in the right half of Figure 3a. The magnetic field at the target surface is of the order of 0.13 T at the radial position where it is parallel to the target ($r = 12.5$ mm). The electron trapping and hopping around the magnetic field lines is clearly

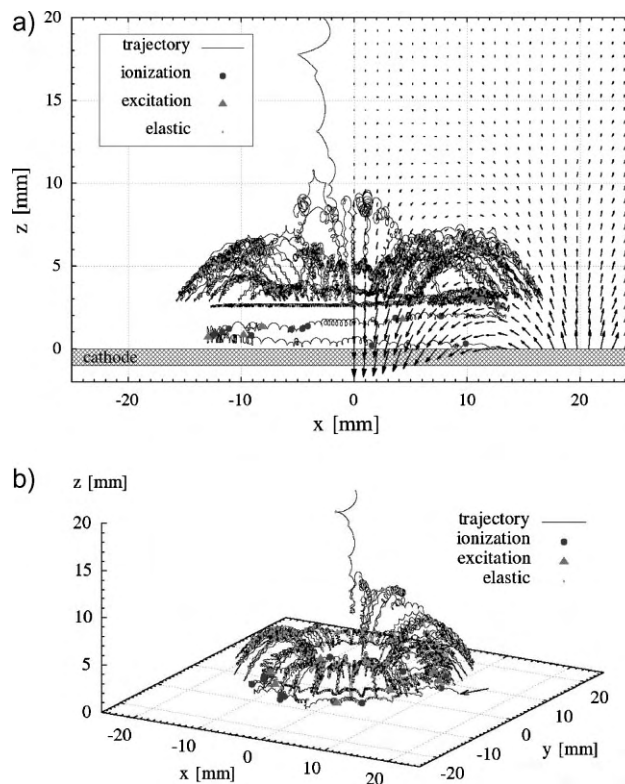


Figure 3. Calculated trajectory of one electron, emitted from the cathode of a direct current magnetron discharge, operating in pure Ar at 10 Pa, a) side view, b) perspective view. The magnetic field lines, as calculated by the Open Source finite element solver GetDP,^[11] are indicated in the right half of Figure 3a. The collisions carried out by the electron are visualized with red full circles (ionization), blue rectangles (excitation) and green dots (elastic collisions). The position where the electron is emitted from the cathode is indicated in Figure 3b by a small arrow.

visible. When the electrons reach the target again, they can be recaptured or reflected. The present example is for pure Ar gas at a pressure of 10 Pa. This value is significantly higher than in typical magnetron discharges, but it is adopted here to illustrate the trajectory and the effect of collisions. Only electron impact ionization, excitation and elastic collisions with Ar atoms are taken into account. These collisions are indicated in Figure 3a and b by red full circles, blue triangles and green dots, respectively. The electron is tracked until it exits the computational volume. In the present example, the test electron stays for 1.63 μs (physical time) in the computational volume, after emission from the cathode until the exit, and it induces 13 ionizations, 7 excitations of argon atoms and it undergoes 884 elastic collisions. A typical ionization distribution, caused by 50 000 electrons, for a pure Ar discharge at a pressure of 0.8 Pa (i.e., more characteristic for magnetrons), is presented in Figure 4. In this case, the electrons are tracked until their total energy (i.e., sum of potential and kinetic energies) drops below 11.5 eV, in order to save

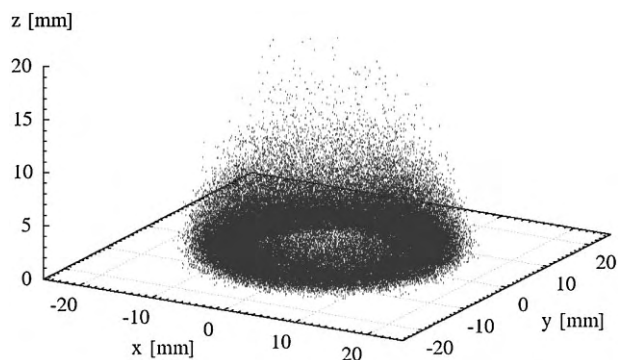


Figure 4. Calculated distribution of ionization collisions of 50 000 electrons, in a direct current magnetron discharge, operating in pure Ar at 0.8 Pa.

computation time. Indeed, electrons with lower energy do not contribute to ionization and excitation collisions and their role as fast electrons is of minor importance. In real time, it takes typically 4 h of computation time to follow these 50 000 electrons on a normal PC. As mentioned above, when the electrons reach the target, they can either be recaptured or reflected. Exact values for the reflection coefficient are not known, but assuming a value of 0.5, it was found that most electrons are quickly recaptured at the cathode. Typically only 5% of the simulated electrons induce collisions and contribute to the ionization in the plasma. It is obvious that most ionization takes place in a ring shape, which corresponds to the magnetic field distribution, i.e., in the area where the magnetic field is parallel to the target surface. Consequently, at these positions, the ion density and flux toward the cathode will reach a maximum, giving rise to enhanced sputtering. The calculated erosion profile (i.e., depth normalized to the maximum depth), as determined from the projection of the ionization distribution on the cathode, is illustrated in Figure 5. By doing this projection we assume that ions are not influenced by the magnetic field and strike the cathode at the same radial position as their position of formation. The calculated erosion profile appears to be in good correlation with the measured normalized erosion profile, as indicated in Figure 5 by the solid line. This example shows the power of MC simulations for describing the detailed electron behavior. Typical calculation times are a few hours, which is very reasonable, certainly in comparison to particle-in-cell–Monte Carlo collision (PIC-MCC) simulations (see below). However, this method is not a self-consistent simulation method, as the electric field distribution needs to be used as input in the model, and is not calculated self-consistently as a result of the charge density distribution. It can, for instance, be obtained from analytical formulas,^[13] or from other calculations, such as PIC-MCC simulations, which are a self-consistent simulation method, as will be explained below.

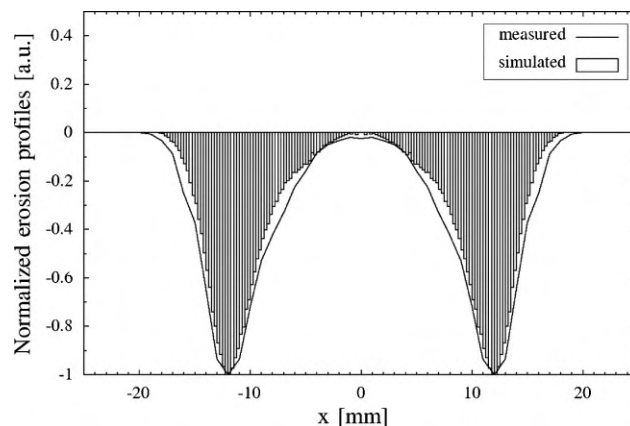


Figure 5. Calculated normalized erosion profile, obtained from Figure 4, by projection of the ionization distribution onto the target, and comparison with the measured normalized erosion profile.

Particle-in-Cell–Monte Carlo Collisions (PIC-MCC) Simulations

Particle-in-cell–Monte Carlo collisions (PIC-MCC) simulations are based on the same principle as MC simulations, i.e., the trajectory of a large number of individual species is calculated using Newton's laws, whereas their collisions are treated with random numbers. However, in PIC-MCC simulations, the electric field distribution is also calculated self-consistently from the positions of the charged species. For this purpose, the positions of the species are projected onto a grid, to obtain a charge density distribution, from which the electric field distribution can be calculated with Poisson equation. However, describing in detail the charged species behavior together with solving the Poisson equation requires a long calculation time. In order to reduce the computation time, the real particles (i.e., electrons and ions) are replaced by a number of so-called super-particles, with a weight corresponding to the number of real particles which they represent. Nevertheless, calculation times can still rise to several weeks for describing magnetron discharges, certainly when some plasma chemistry is included, such as for reactive sputter-deposition applications. The example illustrated here is a PIC-MCC simulation applied to a planar dc magnetron, operating in an Ar/N₂ gas mixture with Ti target (cathode), used for the reactive sputter-deposition of TiN_x films.^[14,15] In this case, beside electrons also several types of ions (Ar⁺, N₂⁺, N⁺, Ti⁺) and fast atoms (Ar_f, Ti_f, N_f) are described in the PIC-MCC model. The fast Ar atoms are created from elastic (including charge transfer) collisions of the Ar⁺ ions with the Ar gas. The fast Ti and N atoms are formed by sputtering, and are followed in this model until they are thermalized. Their further behavior, once thermalized, is described with a diffusion equation, including several production and loss terms (e.g., ionization). Details of this

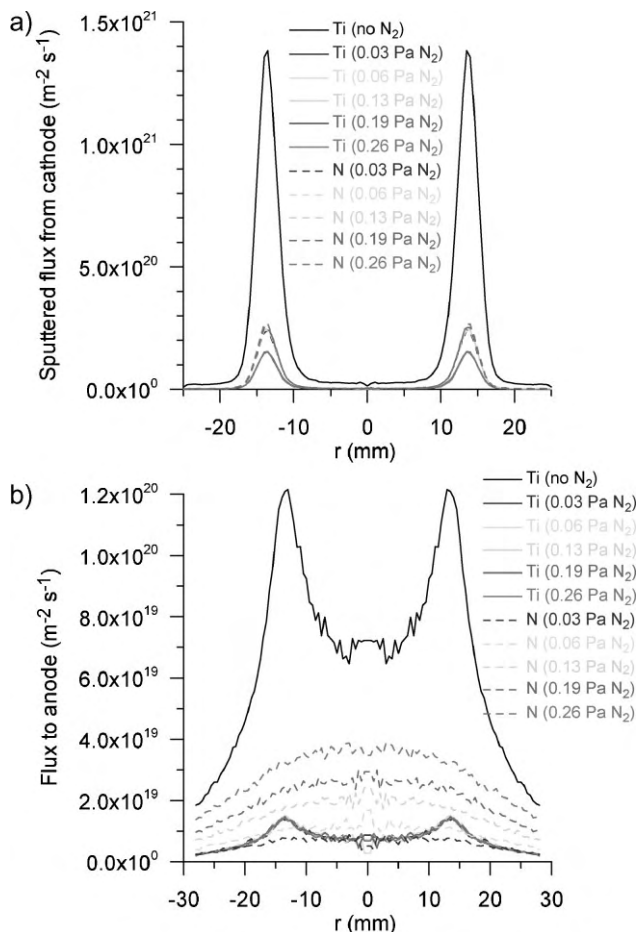


Figure 6. Calculated sputtered fluxes from the cathode a) and fluxes to the anode b), as a function of radial position on the cathode and anode, for both Ti (solid lines) and N (dashed lines) atoms, at different partial pressures of N_2 . The Ar partial pressure is 1 Pa.

model can be found in.^[14] Figure 6a illustrates the calculated fluxes of sputtered Ti and N atoms from the target, as a function of radial position, for pure Ar gas (1 Pa) and for several different partial pressures of N_2 added to the (1 Pa) Ar gas. It is clear that the sputtering occurs mainly at a radial position between 10 and 15 mm from the center, where the magnetic field is parallel to the target. This corresponds to the racetrack, which was also illustrated in Figure 5 above. In pure Ar, there is of course only sputtering of Ti. Upon addition of N_2 to the Ar gas, the sputtered Ti flux drops significantly. This is a consequence of the poisoning of the Ti target, i.e., once N_2 is added to the Ar gas, it will react with the Ti target (through chemisorption and implantation), giving rise to a TiN_x layer on the target, which changes (among others) the sputtering yield of Ti. Möller and Güttler^[16] calculated that the sputtering yield of Ti drops by a factor of 6.4 compared to the sputter yield of Ti from a metallic matrix. This explains the lower sputtered flux. However, once the

target is poisoned (which occurs already at 0.03 Pa partial pressure of N_2), the sputter yield of Ti will not change anymore upon further addition of N_2 to the Ar gas, and therefore the sputtered Ti flux remains more or less constant, as is seen in Figure 6a. The sputter yield of N from the TiN_x target is slightly higher than the corresponding sputter yield of Ti,^[16] and this explains why the sputtering flux of N is about 50% higher than the Ti sputtering flux. It increases slightly upon addition of N_2 gas, because the N^+ and N_2^+ ion concentrations increase, and they give rise to more efficient sputtering of N than the Ar^+ ions.

The sputtered Ti and N atoms pass through the plasma and can be deposited on the substrate, which is located opposite to the target, in the magnetron under study.^[17] Furthermore, not only sputtered N atoms, but also N atoms created in the reactor, for example by dissociation of the N_2 gas, can be deposited on the substrate. It is assumed that the sticking coefficient of N_2 molecules is negligible, so that the N_2 molecules do not contribute to film deposition.^[14] Figure 6b depicts the fluxes of Ti and N atoms on the substrate, as a function of radial position, for the same conditions as in Figure 6a. Again, the flux of Ti atoms is largest, in the pure Ar case, and it drops upon addition of N_2 gas, similar to the behavior of the sputtered Ti atoms. Moreover, the shape of the Ti flux at the substrate also resembles the shape of the sputtered Ti flux, with a maximum at a radial position between 10 and 15 mm from the center. However, the maximum is not so pronounced, and the profile is more spread out, due to diffusion of the sputtered atoms through the plasma. For the N atoms, the peak has disappeared, because most of the N atoms do not originate from the target, but from plasma reactions. Furthermore, it is clear that the N flux increases when more N_2 gas is added, as expected. Based on the sticking coefficients for N and Ti atoms, information can be obtained on the stoichiometry of the deposited TiN_x film. Assuming a sticking coefficient of 1 for N atoms,^[16] and of 0.5 for Ti atoms,^[18] the fluxes presented in Figure 6b would give rise to a stoichiometry x much larger than one. However, in ref. [19] deposited TiN_x films were analyzed with x values in the range 0.26–1.5. This implies that the assumed sticking coefficient of N might be much smaller than 1,^[19] and it will probably even be a function of the coverage of N atoms in the film.^[16] In future work, we would like to investigate this in more detail, by coupling a surface model to our PIC-MCC model.

Hybrid Monte Carlo–Fluid Modeling Network

The above PIC-MCC model can give a detailed, self-consistent and accurate picture of the plasma, taking into account the non-equilibrium behavior of the plasma

Table 1. Overview of the species taken into account in the hybrid model, and the models used to describe their behavior.

| Species | Model |
|--|---|
| Ar atoms | No model (assumed uniform + thermal) or: Gas heat conduction equation or: Gas flow calculation (fluid dynamics) |
| Fast electrons | MC model |
| Slow electrons | Fluid model |
| Ar ⁺ ions | Fluid model MC model in sheath region |
| Fast Ar _f atoms | MC model in sheath region |
| Ar atoms in excited levels | Collisional-radiative model |
| Cu sputtering | Empirical formula + flux energy equations |
| Cu thermalization | MC model |
| Thermal Cu atoms, Cu*, Cu ⁺ , Cu ⁺⁺ , Cu ²⁺ | Collisional-radiation model |
| Cu ⁺ ions | MC model in sheath region |

species. However, as mentioned above, it requires a very long calculation time. Another modeling approach to obtain a self-consistent and detailed picture of the plasma, but at a reduced calculation time, is a so-called hybrid model. By combining different models for different species (e.g., MC simulations for energetic plasma species, which are not in equilibrium with the electric field, such as fast electrons and ions in the sheath region; and fluid models for thermal plasma species, such as neutrals, and ions in the bulk plasma), the calculation time is reduced, but the non-equilibrium plasma behavior is still accounted for. The capabilities of this modeling approach are illustrated here for a dc glow discharge, used for analytical spectrochemistry applications, where the material to be analyzed serves as the cathode (target) of the glow discharge, and is subject to sputtering.^[20,21] The sputtered atoms arrive in the plasma, where they can be ionized and/or excited. The corresponding ions can be measured in a mass spectrometer, whereas the excited atoms emit characteristic photons, which can be detected with optical emission spectrometry. For this purpose, not only electrons, various ions and atoms are included in the model, but also excited atoms and ions. Table 1 gives an overview of the different species that have been included in the hybrid modeling network and the corresponding models used to describe their behavior. As indicated, the Ar atoms can simply be considered to be thermal and uniformly distributed in the plasma, but on the other hand, the calculation of gas heating, as well as the gas flow have also been coupled to this hybrid model, by means of a heat conduction equation^[22] and by computational fluid dynamics simulations,^[23] respectively. Both models give rise to a non-uniform gas density distribution, as illustrated in refs. [22,23]

The electrons are split up in two groups: the so-called fast electrons, with energy above the threshold for inelastic collisions, which are treated with a MC model,^[24] whereas the slow electrons are described with a fluid model.^[25] Indeed, the slow electrons do not have to be described with a MC model, as they cannot give rise to inelastic collisions; their role in the plasma is to provide negative space charge and to carry the electrical current, which can as well be described with a fluid model. The Ar⁺ ions are also treated in this fluid model, and the continuity and transport equations of electrons and ions are coupled to the Poisson equation, in order to obtain a self-consistent electric field distribution. Furthermore, the Ar⁺ ions are also described with a MC model in the sheath region, where a strong electric field is present.^[24,26] In this way, the full ionic energy distribution at the cathode can be obtained, which is needed to calculate the sputtering process. For the same reason, also the fast Ar atoms, which are created from the Ar⁺ ions by elastic (including charge transfer) collisions, are handled with a MC approach in the sheath region, because they also contribute to sputtering.^[24,26,27] The behavior of Ar atoms in excited levels is described with a collisional-radiative model.^[28] This is actually a kind of fluid model, consisting of a set of continuity (or balance) equations (one for each level), with different production and loss terms, such as electron impact (de)excitation, ionization, recombination, radiative decay, etc. More information can be found in ref. [28]. The sputtering process is approximated with an empirical formula for the sputtering yield,^[29] multiplied with the flux energy distributions of the various species bombarding the cathode, calculated in the MC models. This yields the flux of sputtered atoms (in this example Cu). The sputtered atoms have typical energies of several eV, which

they lose rapidly by collisions in the plasma, until they are thermalized. This is described with a MC model.^[30] The further behavior of the sputtered atoms, i.e., transport by diffusion, as well as ionization and excitation, and the behavior of the corresponding ions and atoms in excited levels, is described again with a collisional-radiative model.^[31] Finally, the behavior of the Cu^+ ions in the sheath region is again described with a Monte Carlo model, because the Cu^+ ions also contribute to sputtering.^[27] All these models are coupled to each other due to the interaction processes between the various species, and they are solved iteratively until final convergence is reached. This takes typically several days, which is significantly shorter than in the PIC-MC model described above. Furthermore, the model can easily be extended to also include other species, such as H_2 or N_2 impurities.^[32,33] Typical calculation results include the electrical characteristics (i.e., current-voltage-pressure relationships, electric field and potential distributions), densities, fluxes and energies of the various plasma species, and information about their collisions in the plasma. All these quantities can be obtained as a function of position in the plasma.^[20,21] Results of interest for the applications include the erosion rates and crater profiles at the cathode (i.e., material to be analyzed) due to sputtering, as well as optical emission intensities.

Figure 7a illustrates a calculated crater profile for the so-called VG9000 glow discharge cell, after 1 h of sputtering at 1 000 V, 75 Pa and 3 mA.^[34] It should be mentioned that this analytical glow discharge is not only used for bulk

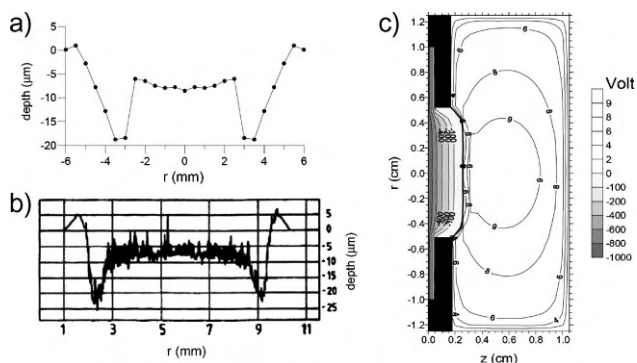


Figure 7. Calculated a) and measured b) crater profiles at the cathode, obtained after 1 h of sputtering in the so-called VG9000 glow discharge cell, at 1 000 V, 75 Pa and 3 mA. Also shown is the two-dimensional electric potential distribution for the same conditions c), illustrating that the equipotential lines are not completely parallel to the cathode surface. The cathode is located at the left border of the Figure, whereas the other Figure borders represent the anode cell walls. The black rectangles between $z=0$ and $z=0.05$ cm symbolize the insulating ring between cathode and anode, and the black rectangles between $z=0.05$ cm and $z=0.15$ cm represent the so-called front plate at anode potential.

analysis of materials, but also for so-called depth profiling, i.e., measuring the impurity concentrations in the sample as a function of depth. For this purpose, it is of course important to obtain flat crater profiles, so that impurities at a certain depth are sampled at the same moment in time. It is clear that the calculated crater profile depicted in Figure 7a is far from ideal for depth profiling analysis. Indeed, the crater is much deeper at the sides than in the center. This so-called “crater edge effect” is also found back in the measured crater profile, as illustrated in Figure 7b, which was obtained for exactly the same conditions. The reason for this effect can be understood, when looking at the potential distribution in this glow discharge cell, as shown in Figure 7c. Indeed, this cell is characterized by an anode plate in front of the cathode (visualized with the black rectangles in Figure 7c), to limit the cathode-sputtering to a certain part of the sample. However, as a consequence, the equipotential lines are not completely flat in front of the cathode, and the ions bombarding the cathode are preferentially focused to a radial position of 0.4 cm from the cell axis, yielding more sputtering, and hence a deeper crater than in the center. This demonstrates that the VG9000 glow discharge cell is not well suitable for depth profiling analysis, unless some modifications are proposed, as discussed in ref. [34]

Another glow discharge cell, which is very often used for chemical analysis applications, is the so-called Grimm-type cell. In Figure 8a and b some calculated and measured crater profiles are plotted. They were both obtained for 157 s of sputtering, at 880 V and 5 mA.^[35] It is clear that these craters are much more flat, which can be understood when looking at the potential distribution in front of the cathode, visualized in Figure 8c. Indeed, the equipotential lines are now much more parallel to the cathode surface, and therefore this Grimm-type cell is clearly more suitable

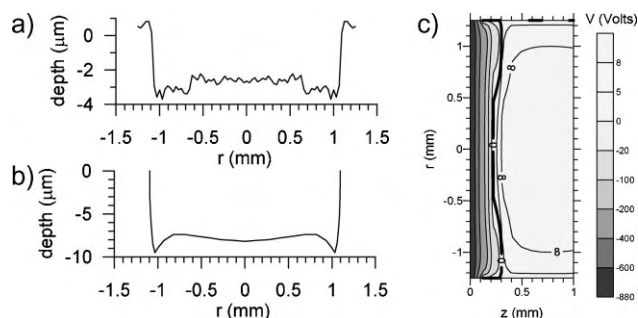


Figure 8. Calculated a) and measured b) crater profiles at the cathode, obtained after 157 s of sputtering in the so-called Grimm-type cell, at 880 V and 5 mA. Also shown is the two-dimensional electric potential distribution for the same conditions c). Note that the Grimm-type cell is much longer than shown in Figure 8c, but only the first mm in front of the cathode is presented, to illustrate a detailed view of the equipotential lines in front of the cathode.

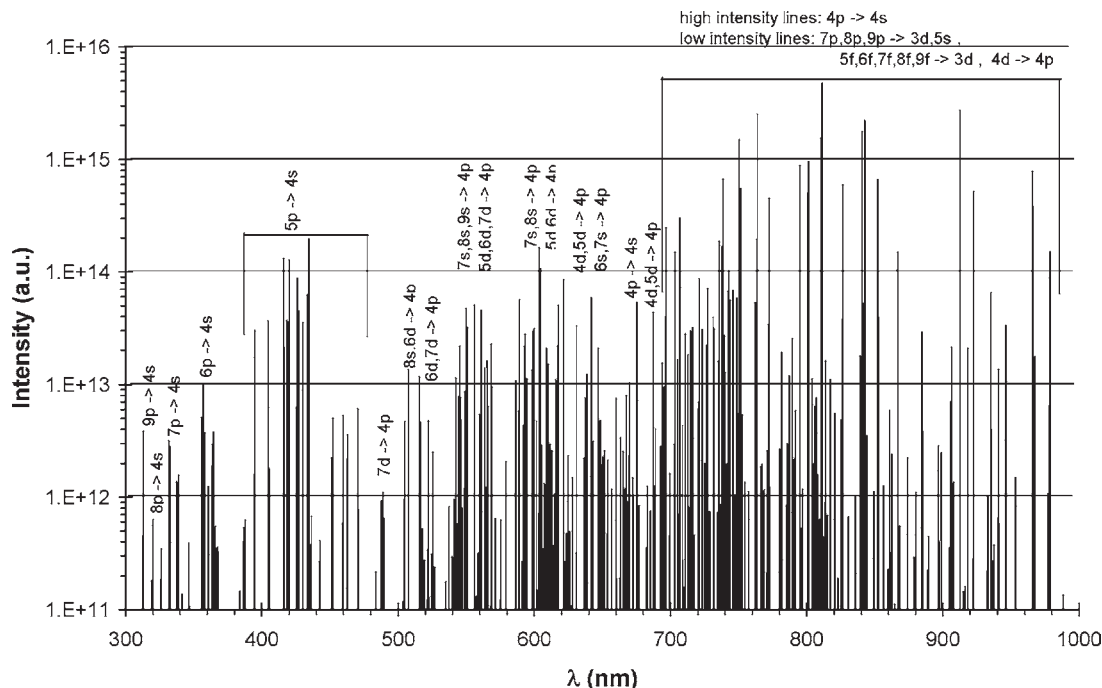


Figure 9. Calculated optical emission spectrum of the Ar(I) lines (605 in total), for the conditions of 1 000 V, 133 Pa and 2 mA (adopted from ref. [21] with kind permission of the Royal Society of Chemistry).

for depth profiling analysis, as is demonstrated by the large number of publications on this topic (see e.g.^[36–38]). This example shows how a result of analytical interest can be understood and interpreted, and possibly improved, based on investigations of the basic plasma behavior.

Another important calculation result, from applications point of view, is the optical emission spectrum, which can be obtained from the populations of the excited levels, as calculated in the collisional-radiative models. Figure 9 illustrates the calculated spectrum of Ar(I) lines, for typical operating conditions of 1 000 V, 133 Pa and 2 mA.^[39] In total, 605 lines are taken into account. It is clear that the 4p–4s lines in the region 700–1 000 nm have the highest intensity, followed by the 5p–4s lines, in the region 400–500 nm. This spectrum agrees qualitatively with a spectrum found in the literature for a hollow cathode glow discharge,^[40] demonstrating that the collisional-radiative model takes into account the correct processes. This was also illustrated in ref. [41], where the calculated axial profiles of several Ar(I), Ar(II) and Cu(I) lines were compared with experimental data, for a wide range of operating conditions.

Molecular Dynamics Simulations

Modeling the plasma behavior is of interest for improving the various applications, but besides the processes in the

plasma, the interaction with the walls is also of great importance, for two major reasons: (i) it forms the basis of many applications, such as plasma deposition, etching, surface modification, etc., and (ii) it determines the boundary conditions of the plasma simulations. Plasma-surface interactions can be modeled in a macroscopic way, based on surface reaction probabilities, sticking coefficients, etc., e.g., etch profile simulations,^[42] but these reaction coefficients then need to be obtained from experiments or from detailed atomistic simulations, such as molecular dynamics (MD) modeling. The latter modeling approach can also provide detailed information on the reaction mechanisms at the surface, and on the resulting microscopic structure of deposited films, as it will be shown below.

The principle of MD simulations is based on following the temporal behavior of all atoms in a system (i.e., individual atoms in the substrate and atoms belonging to plasma species arriving at the substrate) by Newton's laws. The force acting on the various atoms is obtained from the interatomic interaction potential between all atoms. Hence, the system can be described in a fully deterministic way. However, the reliability of the results depends greatly on the choice of this interaction potential. In classical MD simulations, mostly empirical potentials are applied, for which the parameters are obtained by fitting to experiments or to density-functional-theory. We have applied this MD approach to the plasma

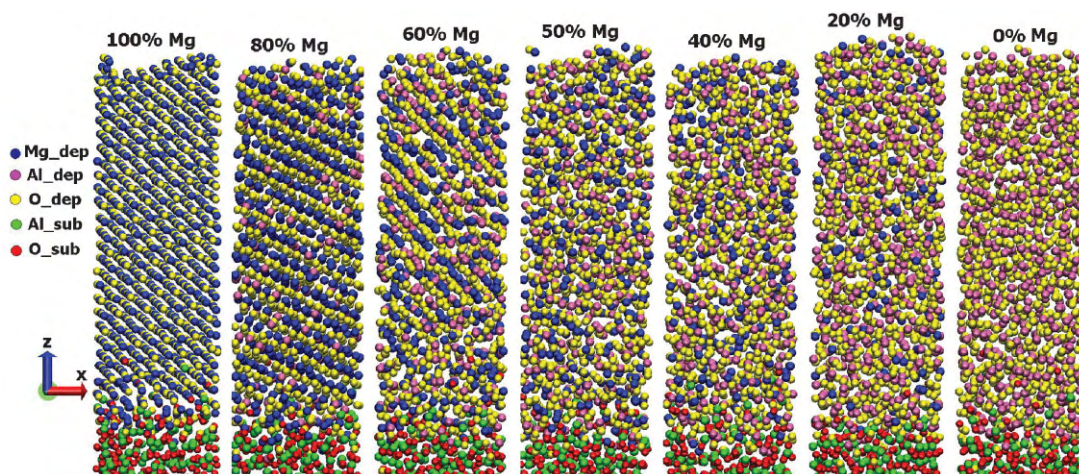


Figure 10. Calculated microscopic structures of deposited $\text{Mg}_x\text{Al}_y\text{O}_z$ films on an amorphous Al_2O_3 substrate, for conditions typical for dual magnetron reactive sputter-deposition. The different colors represent different kinds of atoms, as indicated by the legend. The impacting atoms are Mg, Al and O, at different ratios. The Mg content, relative to the total metal flux (Mg + Al), is indicated above each structure (adopted from ref. [47] with kind permission of IOP Publishing).

deposition of metal oxide thin films, based on classical pair-wise ionic potentials,^[43] and to various carbon systems (amorphous carbon, diamond-like carbon, nanocrystalline diamond, carbon nanotubes), where we apply the so-called Brenner potential,^[44] or a modified version, developed by Shibuta and Maruyama, for carbon nanotube growth (interaction between carbon and metal nanoparticles).^[45,46]

Figure 10 illustrates the calculated microscopic structure and the composition of thin $\text{Mg}_x\text{Al}_y\text{O}_z$ films, deposited on an amorphous Al_2O_3 substrate by dual magnetron reactive sputter-deposition, for different ratios of Mg and Al fluxes.^[47] In order to limit the calculation time, the simulation box is limited to a surface area of $17 \times 17 \text{ \AA}^2$. The film is grown to a thickness of approximately 5 nm. The simulation time per impact is 2 ps, followed by 2 ps of relaxation, before the next impact takes place. This yields far too high deposition rates, but it is required to limit the calculation time. In reality, the film will relax during a much longer time (order of μs) before the next impact takes place, enabling surface diffusion and other relaxation processes. However, such long simulation times are not feasible with MD simulations; for this purpose, acceleration techniques, such as accelerated molecular dynamics methods,^[48] activation-relaxation techniques,^[49] or MC simulations^[50] need to be applied. Nevertheless, in the case of magnetron sputter-deposition, where the growth process is assisted by energetic ion bombardment, thermal surface diffusion probably does not play a significant role in the film growth if the substrate temperature is low compared to the activation energy barrier for surface diffusion.^[51] As observed in Figure 10, the growing film appears to be crystalline when

the Mg to Al flux ratio to the substrate is large, and it gradually becomes an amorphous structure when more Al than Mg is deposited. This simulation result was also found for film growth on crystalline substrates, and it was also confirmed by X-ray diffraction and transmission electron microscopy experiments, as is explained in detail in ref. [47]. The reason for this transition from a crystalline to an amorphous structure is probably related to the fact that the crystal structures of MgAl_2O_4 and Al_2O_3 are more complex than the simple cubic crystal structure of MgO, yielding a much more complex energy surface when the Al concentration increases, so that surface diffusion, giving rise to crystallization of the film, is less obvious. Further studies of the activation energy barriers and diffusion coefficients are foreseen in order to investigate these mechanisms in more detail.

MD simulations can also provide better insight in the growth mechanisms of amorphous carbon films. Figure 11 illustrates the effect of hydrogen on the calculated mass and atom densities in a growing hydrogenated amorphous carbon film.^[52] It was found that the incorporation of H into the film increases the mass density, up to a H content (or H-flux) of about 10%. The atom density of the films reaches a maximum at a H-content of about 22%. It was demonstrated in ref. [52] that these effects are a result of the change in the microstructure of the films, including a H-induced sp^2 to sp^3 shift. Experimentally, a H content of about 33% and a mass density of about $1.5 \text{ g} \cdot \text{cm}^{-3}$ were found, which corresponds well with our simulations. The results show how amorphous hydrogenated carbon films can be densified using low H-fluxes to the substrate, for instance when no ion bombardment densification is possible.^[52]

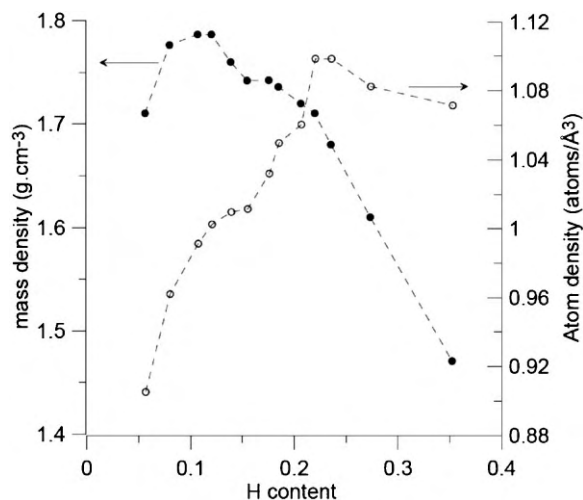


Figure 11. Calculated mass density (left axis, full circles) and atom density (right axis, open circles) as a function of H content in an amorphous hydrogenated carbon film, deposited from hydrocarbon radicals at thermal energy (adopted from ref. [52] with kind permission of American Institute of Physics).

Finally, the relative importance of impacting species to the growth process can also be deduced from MD simulations, based on calculated sticking coefficients. Figure 12a and b illustrates the calculated sticking coefficients of the various CH_x ($x=0-4$) and C_2H_x ($x=0-6$) species, respectively, bombarding a diamond substrate. The reaction behavior was investigated on the two most important crystallographic diamond surfaces with reconstruction geometries corresponding to the hydrogenated surfaces, i.e., $(100)2 \times 1$ and $(111)1 \times 1$, and for two different temperatures, i.e., 800 and 1100 K, which are characteristic for the growth of ultra-nanocrystalline diamond (UNCD) and nanocrystalline diamond (NCD) thin films, respectively.^[53,54] It appears from Figure 12 that the sticking behavior of the various impacting species was very similar for the two different diamond surfaces, and the two different temperatures, although the diamond $(111)1 \times 1$ surface exhibited a slightly more pronounced temperature variation than the diamond $(100)2 \times 1$ surface. In general, a significant drop in the sticking coefficients is predicted, both in the series $\text{C}-\text{CH}_4$, and the series $\text{C}_2-\text{C}_2\text{H}_6$. This is certainly correlated with the number of free electrons in the species, as is indicated on the top axes, which is logical because these free electrons can form bonds to the surface. Nevertheless, the drop in sticking coefficient does not show a completely linear variation with

the number of free electrons, indicating that there must be a second effect, attributed to sterical hindrance caused by H-atoms bound to the impacting C-atoms. Indeed, these H-atoms cause shielding of the C-atoms, preventing their sticking efficiency at the surface.

Beside the overall sticking efficiency, also the resulting coordination of the C-atoms is important, because this determines whether the impacting species contribute to the growth of the diamond structure. This is investigated in detail in ref. [54] Moreover, surface relaxation can be important to promote the growth of diamond structures. However, as mentioned above, these surface relaxation and diffusion processes cannot be described by classical MD simulations, because of the limited calculation time. For this purpose, we have recently developed a Metropolis MC algorithm,^[55] to couple to the MD model, in order to account for surface relaxation, and to investigate in more detail the plasma deposition of (U)NCD films.^[56]

Conclusion

Some examples of modeling activities, currently going on in our research group, are presented, illustrating the strengths and limitations of the various modeling approaches. This is also summarized in Table 2. A fluid model, based on solving continuity and transport equations for the various plasma species, is particularly suitable for describing the detailed plasma chemistry. Indeed, a large number of different species and chemical reactions can be included in the model, without too much computational effort. By coupling the continuity equations of the charged plasma species to the Poisson equation, the electric field distribution can be self-consistently obtained. However, this approach is not so

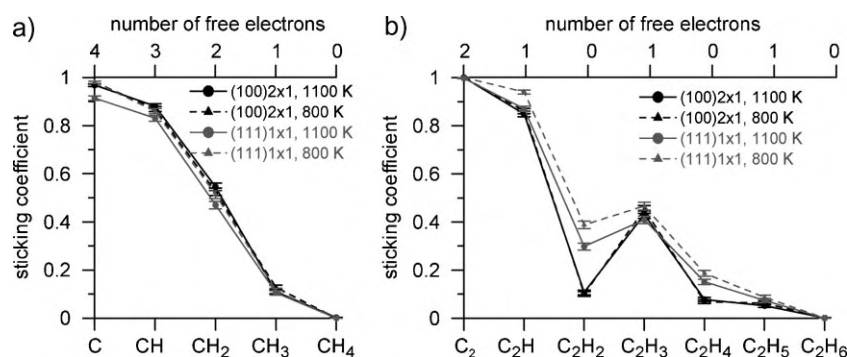


Figure 12. Calculated sticking coefficients of CH_x species ($x=0-4$) (a) and C_2H_x species ($x=0-6$) (b) on the two most important crystallographic diamond surfaces with reconstruction geometries corresponding to the hydrogenated surfaces (i.e., diamond $(100)2 \times 1$ and diamond $(111)1 \times 1$), for two different substrate temperatures, which are relevant for the growth of nanocrystalline and ultranancrystalline diamond films (i.e., 1100 and 800 K, respectively), as indicated by the legends. The top axes represent the number of free electrons in the various CH_x and C_2H_x species.

Table 2. Summary of the various models for describing plasmas or plasma-surface interactions, explained in this paper, with their strengths and limitations. Note that there exist other modeling approaches in literature as well, such as analytical models, or solving the Boltzmann equation, but they are not included in this table, as we have no experience with them in our research group.

| Model | Short description | Strengths | Limitations |
|----------------------------------|--|---|--|
| Fluid | Continuity + transport equations for all plasma species + Poisson equation for electric field | - Fast - Detailed plasma chemistry - Self-consistent | - Approximation (for non-equilibrium electron behavior) |
| Monte Carlo | Newton's laws for species' trajectory + random numbers for collisions | - Suitable for non-equilibrium electron behavior | - Not self-consistent |
| PIC-MCC | Similar to MC + Poisson equation for electric field | - Suitable for non-equilibrium electron behavior - Self-consistent | - Long calculation time |
| Hybrid | Combination of several models (e.g., fluid + MC) | - Suitable for non-equilibrium electron behavior - Self-consistent - Reduced calculation time compared to PIC-MCC | - Still rather long calculation time |
| MD (plasma-surface interactions) | Newton's laws for atom behavior, based on interatomic interaction potential | - Detailed + accurate description on atomistic level - Self-consistent | - Very long calculation time - Accuracy critically depends on choice of interatomic interaction potential |

suitable for describing the detailed (and non-equilibrium) electron behavior, as only the average electron energy is calculated by an energy balance equation. The detailed electron behavior can be simulated very accurately by MC simulations, which are based on solving Newton's laws for the electron trajectory and random numbers to treat their collisions; however, this approach on its own is not a self-consistent simulation method. This problem can be overcome by integrating the MC method in a PIC-MCC simulation, where the description of the plasma species trajectory and collisions is coupled to solving the Poisson equation, in order to obtain a self-consistent electric field distribution. The major disadvantage of this approach is, however, the long calculation time. An alternative for PIC-MCC simulations is the so-called hybrid approach, which combines several models (e.g., MC and fluid simulations, but also other models, like collisional-radiative models can be added) into a modeling network. In this way, the advantages of the individual models can be combined, whereas the disadvantages can be avoided (although it should be mentioned that the calculation time

can still be rather long). Finally, for modeling plasma-surface interactions, MD simulations are a very powerful tool, as they provide insight in the detailed reaction mechanisms on the atomic scale. Furthermore, based on fluxes from plasma species, obtained from experiments or plasma simulations, the film growth process can be simulated, and the microscopic structure and composition of growing films can be predicted. This paper has illustrated that the most suitable modeling approach depends on the application, and that by combining different modeling approaches, a complete picture of the plasma behavior, including the surface processes, can be obtained.

Acknowledgements: *M. Eckert* is indebted to the *Institute for the Promotion of Innovation by Science and Technology in Flanders (IWT-Flanders)* for financial support. *E. Neyts* acknowledges financial support from the *Fund for Scientific Research Flanders (FWO)*. This work is also supported by a NOI project of the *University of Antwerp*, an FWO project, an IWT (SBO) project and an IAP-VI project of the *Prime Minister's Office*. Finally, the calculation

support of the core facility *CALCUA*, provided by the *University of Antwerp*, is gratefully acknowledged.

Received: November 5, 2008; Revised: December 22, 2008;
Accepted: January 13, 2009; DOI: 10.1002/ppap.200800207

Keywords: computer simulations; fluid modeling; molecular dynamics; particle-in-cell Monte Carlo; plasma modeling; plasma-surface interactions

- [1] Y. T. Lee, M. A. Lieberman, A. J. Lichtenberg, F. Bose, H. Baltes, R. Patrick, *J. Vac. Sci. Technol.* **1997**, *15*, 113.
- [2] J. D. P. Passchier, W. J. Goedheer, *J. Appl. Phys.* **1993**, *73*, 1073.
- [3] D. Loffhagen, F. Sigeneger, R. Winkler, *J. Phys. D: Appl. Phys.* **2002**, *35*, 1768.
- [4] Z. Donko, K. Rozsa, R. C. Tobin, *J. Phys. D: Appl. Phys.* **1996**, *29*, 105.
- [5] M. Surendra, D. B. Graves, *IEEE Trans. Plasma Sci.* **1991**, *19*, 144.
- [6] Z. Donko, *J. Appl. Phys.* **2000**, *88*, 2226.
- [7] M. Mao, J. Benedikt, A. Consoli, A. Bogaerts, *J. Phys. D: Appl. Phys.* **2008**, *41*, 225201.
- [8] Ch. Deschenaux, A. Affolter, D. Magni, Ch. Hollenstein, P. Fayet, *J. Phys. D: Appl. Phys.* **1999**, *32*, 1876.
- [9] K. De Bleecker, A. Bogaerts, W. Goedheer, *Phys. Rev. E* **2006**, *73*, 026405.
- [10] K. Ostrikov, *Rev. Mod. Phys.* **2005**, *77*, 489.
- [11] <http://www.geuz.org/getdp/>
- [12] <http://www.geuz.org/gmsh/>
- [13] Q. H. Fan, L. Q. Zhou, J. J. Gracio, *J. Phys. D: Appl. Phys.* **2003**, *36*, 244.
- [14] E. Bultinck, A. Bogaerts, S. Mahieu, D. Depla, *New. J. Phys.* **2009**, *11*, 023039.
- [15] E. Bultinck, S. Mahieu, D. Depla, A. Bogaerts, *Plasma Proc. Polym.* in press.
- [16] W. Möller, D. Güttler, *J. Appl. Phys.* **2007**, *102*, 094501.
- [17] E. Bultinck, I. Kolev, A. Bogaerts, D. Depla, *J. Appl. Phys.* **2007**, *103*, 013309.
- [18] S. Mahieu, K. Van Aeken, D. Depla, D. Smeets, A. Vantomme, *J. Phys. D: Appl. Phys.* **2008**, *41*, 152005.
- [19] D. Mao, T. J. Hopwood, *J. Vac. Sci. Technol. A* **2002**, *20*, 379.
- [20] A. Bogaerts, *Plasma Sources Sci. Technol.* **1999**, *8*, 210.
- [21] A. Bogaerts, *J. Anal. At. Spectrom.* **2007**, *22*, 13.
- [22] A. Bogaerts, R. Gijbels, V. V. Serikov, *J. Appl. Phys.* **2000**, *87*, 8334.
- [23] A. Bogaerts, A. Okhrimovskyy, R. Gijbels, *J. Anal. At. Spectrom.* **2002**, *17*, 1076.
- [24] A. Bogaerts, M. van Straaten, R. Gijbels, *Spectrochim. Acta, Part B* **1995**, *50*, 179.
- [25] A. Bogaerts, R. Gijbels, W. J. Goedheer, *J. Appl. Phys.* **1995**, *78*, 2233.
- [26] A. Bogaerts, R. Gijbels, *J. Appl. Phys.* **1995**, *78*, 6427.
- [27] A. Bogaerts, R. Gijbels, *J. Appl. Phys.* **1996**, *79*, 1279.
- [28] A. Bogaerts, R. Gijbels, J. Vlcek, *J. Appl. Phys.* **1998**, *84*, 121.
- [29] N. Matsunami, Y. Yamamura, Y. Itikawa, N. Itoh, Y. Kazumata, S. Miyagawa, K. Morita, R. Shimizu, H. Tawara, *At. Data Nucl. Data Tables* **1984**, *31*, 1.
- [30] A. Bogaerts, M. van Straaten, R. Gijbels, *J. Appl. Phys.* **1995**, *77*, 1868.
- [31] A. Bogaerts, R. Gijbels, R. J. Carman, *Spectrochim. Acta, Part B* **1998**, *53*, 1679.
- [32] A. Bogaerts, R. Gijbels, *Spectrochim. Acta, Part B* **2002**, *57*, 1071.
- [33] A. Bogaerts, *Spectrochim. Acta, Part B* **2009**, *64*, 126.
- [34] A. Bogaerts, R. Gijbels, *Spectrochim. Acta, Part B* **1997**, *52*, 765.
- [35] A. Bogaerts, W. Verscharen, E. Steers, *Spectrochim. Acta, Part B* **2004**, *59*, 1403.
- [36] J. Angeli, A. Bengtson, A. Bogaerts, V. Hoffmann, V.-D. Hodoroaba, E. Steers, *J. Anal. At. Spectrom.* **2003**, *18*, 670.
- [37] K. Shimizu, H. Habazaki, P. Skeldon, G. E. Thompson, *Spectrochim. Acta, Part B* **2003**, *58*, 1573.
- [38] V. Hoffmann, R. Dorka, L. Wilken, V.-D. Hodoroaba, K. Wetzig, *Surf. Interface Anal.* **2003**, *35*, 575.
- [39] A. Bogaerts, R. Gijbels, J. Vlcek, *Spectrochim. Acta, Part B* **1998**, *53*, 1517.
- [40] D. E. Gray, "American Institute of Physics Handbook", 3rd ed., McGraw Hill, New York 1972.
- [41] A. Bogaerts, Z. Donko, K. Kutasi, G. Bano, N. Pinhao, M. Pinheiro, *Spectrochim. Acta, Part B* **2000**, *55*, 1465.
- [42] A. Sankaran, M. Kushner, *J. Vac. Sci. Technol. A* **2004**, *22*, 1242.
- [43] C. R. A. Catlow, C. M. Freeman, R. L. Royle, *Physica* **1985**, *131B*, 1.
- [44] D. W. Brenner, *Phys. Rev. B* **1990**, *42*, 9458.
- [45] Y. Shibuta, S. Maruyama, *Comp. Mat. Sci.* **2007**, *39*, 842.
- [46] Y. Shibuta, S. Maruyama, *Chem. Phys. Lett.* **2007**, *437*, 218.
- [47] V. Georgieva, M. Saraiva, N. Jehanathan, O. Lebelev, D. Depla, A. Bogaerts, *J. Phys. D: Appl. Phys.* **2009**, *42*, 065107.
- [48] A. Voter, F. Montalenti, T. Germann, *Annu. Rev. Mater. Res.* **2002**, *32*, 321.
- [49] N. Mousseau, G. T. Barkema, *Phys. Rev. E* **1998**, *57*, 2419.
- [50] L. A. Tabarovsky, M. M. Goldman, M. B. Rabinovich, K.-M. Strack, C. H. Grein, R. Benedek, T. de la Rubia, *Comp. Mat. Sci.* **1996**, *6*, 123.
- [51] P. R. Willmott, *Prog. Surf. Sci.* **2004**, *76*, 163.
- [52] E. Neyts, A. Bogaerts, M. C. M. van de Sanden, *Appl. Phys. Lett.* **2006**, *88*, 141922.
- [53] M. Eckert, E. Neyts, A. Bogaerts, *J. Phys. D: Appl. Phys.* **2008**, *41*, 032006.
- [54] M. Eckert, E. Neyts, A. Bogaerts, *Chem. Vap. Deposition* **2008**, *14*, 213.
- [55] N. Metropolis, A. W. Rosenbluth, M. N. Rosenbluth, A. H. Teller, E. Teller, *J. Chem. Phys.* **1953**, *21*, 1087.
- [56] M. Eckert, E. Neyts, A. Bogaerts, *Cryst. Eng. Commun.* submitted.